modification of the Levitus (1982) data was that the mixed-layer temperature in the sea-ice region was reset to the freezing temperatures calculated from salinity.

As the final stage of the preliminary time integration, a 30 year time integration of the CGCM after initiation with the final states of the AOGCM-run and the OGCM-run was performed. The 1973-1990 average sea-ice concentration, obtained from Joint Ice Center data, was used as the initial condition. The initial sea-ice thickness was estimated as a linear function of the sea-ice concentration with maximum values of 3 m in the Northern Hemisphere and 0.5 m in the Southern Hemisphere. During the integration, the temperature and salinity of the uppermost layer were relaxed to the modified climatological SST and SSS from Levitus (1982). The relaxation terms were averaged over the last 10 years of the integration and their monthly means were stored as heat and freshwater flux adjustment terms (Fig. 7).

Two runs were performed, *i.e.*, a run with the atmospheric CO_2 concentration fixed at 345 ppmv (C run) and a run with a gradual increase in CO_2 at a compound annual rate of 1% (G run). This rate of CO_2 increase corresponds roughly to the actual increase of radiative forcing due to the increases in several greenhouse gases and has been used in other studies (Stouffer *et al.*, 1989; Manabe et al, 1991; Murphy, 1992). In both the C and G runs, the flux adjustments for the surface energy and water fluxes obtained above were included to predict realistic SSTs and SSSs. Both the C and G runs were continued up to year 70.

4 Simulation of the present climate

The performance of the C run is presented in this section.

4.1 SST and meridional circulation

The flux adjustments for the 70 year integration of the model worked well to maintain the calculated annual mean SST close to the Levitus (1982) climatology for the mid-high latitudes as well as for the tropical region (Fig. 8). During the 70 year time integration, however, the model had some climate drift in the subsurface ocean at high latitudes, especially for the Antarctic Ocean and the North Atlantic. The overall features of the SST pattern were reproduced reasonably well. Some

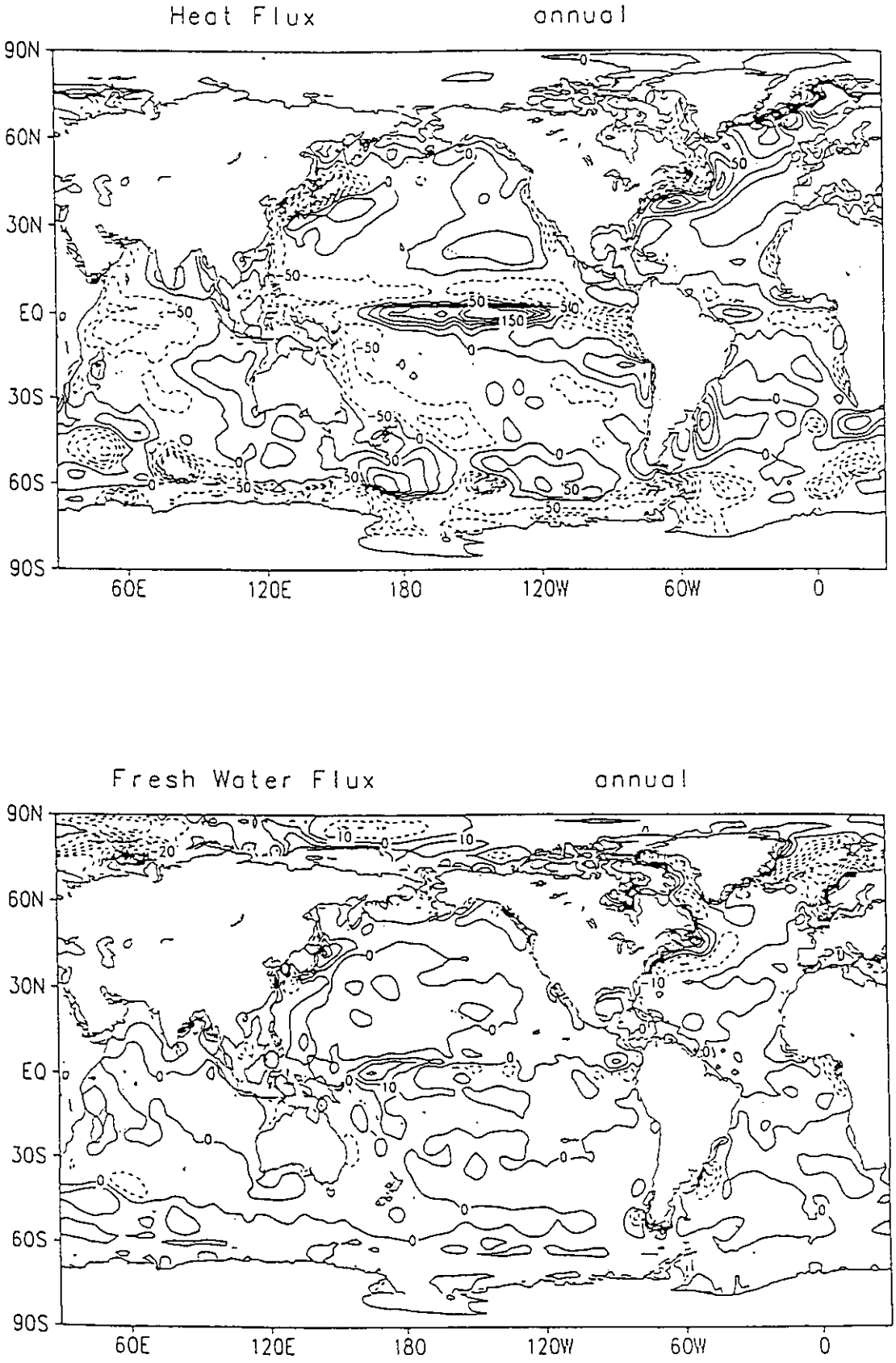

Fig. 7 The annually-averaged geographical distribution of the flux adjustment terms for heat (upper panel) and fresh water (lower panel) used for the C and G runs. Positive values indicate the fluxes from the atmosphere to the ocean.

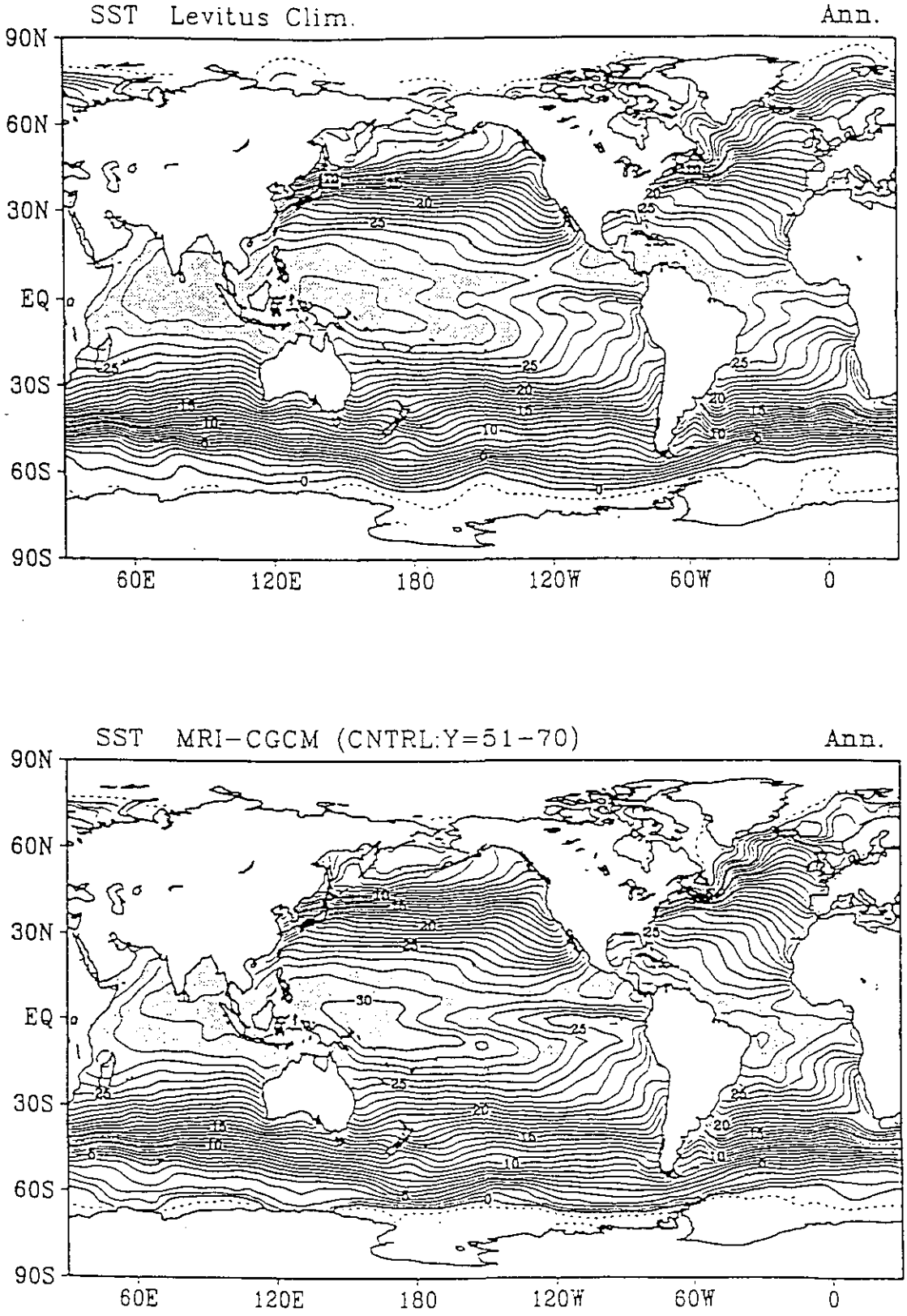

Fig. 8 Observed (upper panel; Levitus, 1982) and model (lower panel) climatologies of annual mean sea surface temperature (SST). Contour interval is 1.°C with shading for temperatures greater than 27 °C.

discrepancies from the observation, however, were seen. The temperature of the western equatorial warm water in the Pacific was slightly higher than 30°C while that observed was less than 30°C. The model SST generally had a warm bias for the warm water regions of the tropics.

The mass stream function of the zonally integrated meridional circulation of the C run (Fig. 9) shows that two shallow overturning cells in the tropics, the Deacon cell between 40° and 60°S and the deep thermohaline cell adjacent to the coast of Antarctica were simulated. However, the thermohaline circulation in the Northern Hemisphere was very weak in this simulation compared with those obtained by other studies (e.g., Manabe *et al.*, 1991; Murphy, 1995 a, b) where peak values of around 15 Sverdrups are typical. This weak overturning is partly caused by the different ocean depth used for the relaxation to the observed SST and SSS between the third stage and the final stage for the ocean spin-up. Since the ocean model used in this study had a very thin surface layer (5.2 m), the positive heat flux adjustments (see Fig. 7), which were required to retain the observed SST in the North Atlantic, may excessively stabilize the upper layers, so that the overturning may become very weak in the final stage for the ocean spin-up.

4.2 Atmospheric fields

The basic atmospheric fields are expected to be rather well simulated in the C run because the flux adjustment worked well to simulate the observed SST (see Fig. 8). Therefore, the main features of the atmospheric climatology were also well simulated. However, common deficiencies were also found between the AMIP simulation by the MRI-AGCM (Kitoh *et al.* 1995) and the C run by the MRI-CGCM. There was a cold bias of about 10 °C over the lower stratosphere with the largest values of more than 20 °C being found at the tropopause level (Fig. 10). This bias was related to the stronger polar night jets (Fig. 11). A cold polar bias was also found in the annual-mean surface air temperature field (Fig. 12). We compared the simulated annual mean sea-level pressure with observations (Fig. 13). The deficiencies of an eastward extension of the Aleutian low toward the continent during winter circulation and the excessive mass in the subtropical and mid-latitude ocean with the compensationally deficient mass over land during summer circulation found in the AMIP simulation (Kitoh *et al.* 1995) were also found in the annual mean field of the C run. The

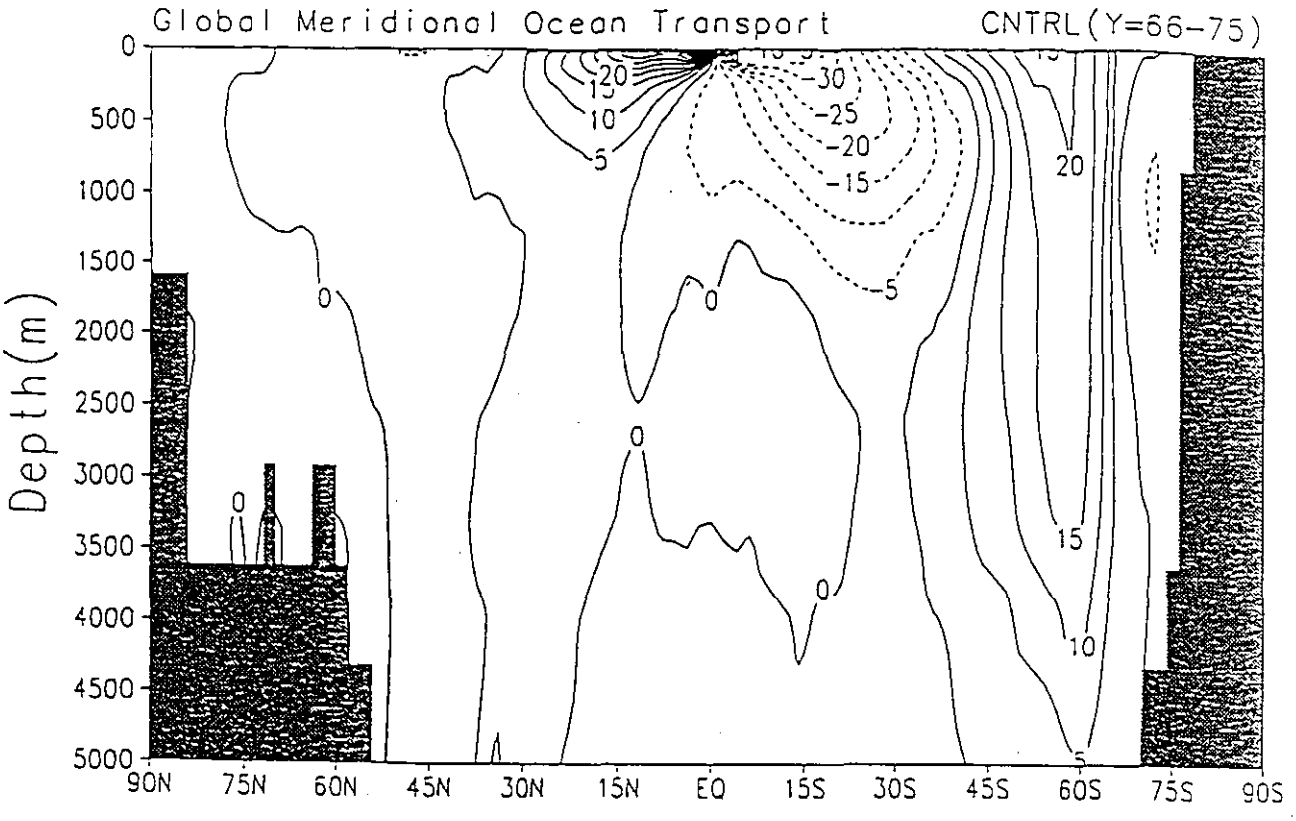

Fig. 9 Latitude-depth distribution of the stream function of the meridional circulation in the global ocean averaged over the last 10 years of the C run. Units are Sverdrups (10^6 m^3s^{-1}).

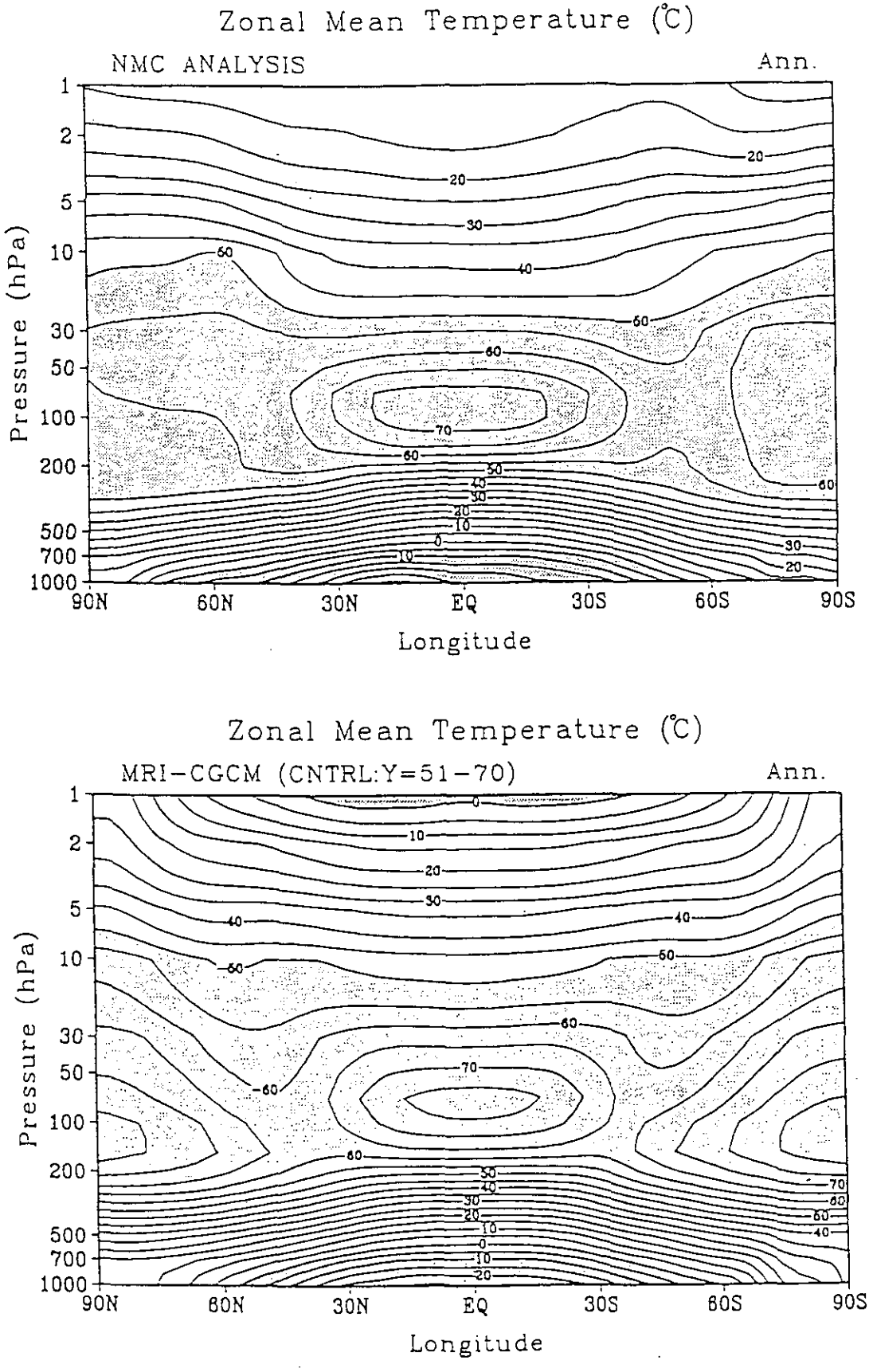

Fig. 10 Latitude-height cross section of zonally-averaged annual-mean temperature for observation from NMC analyses (upper panel) and simulation in the C run (mean of years 51-70) (lower panel). Contour interval is 5 °C.

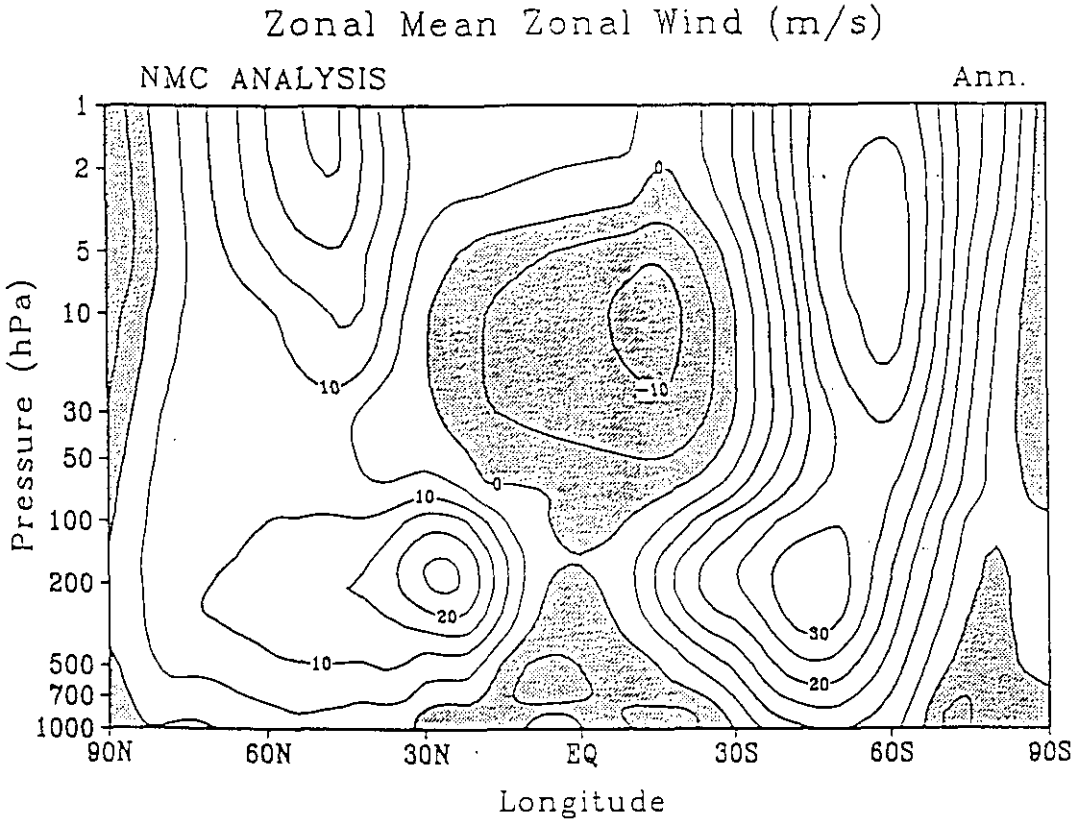

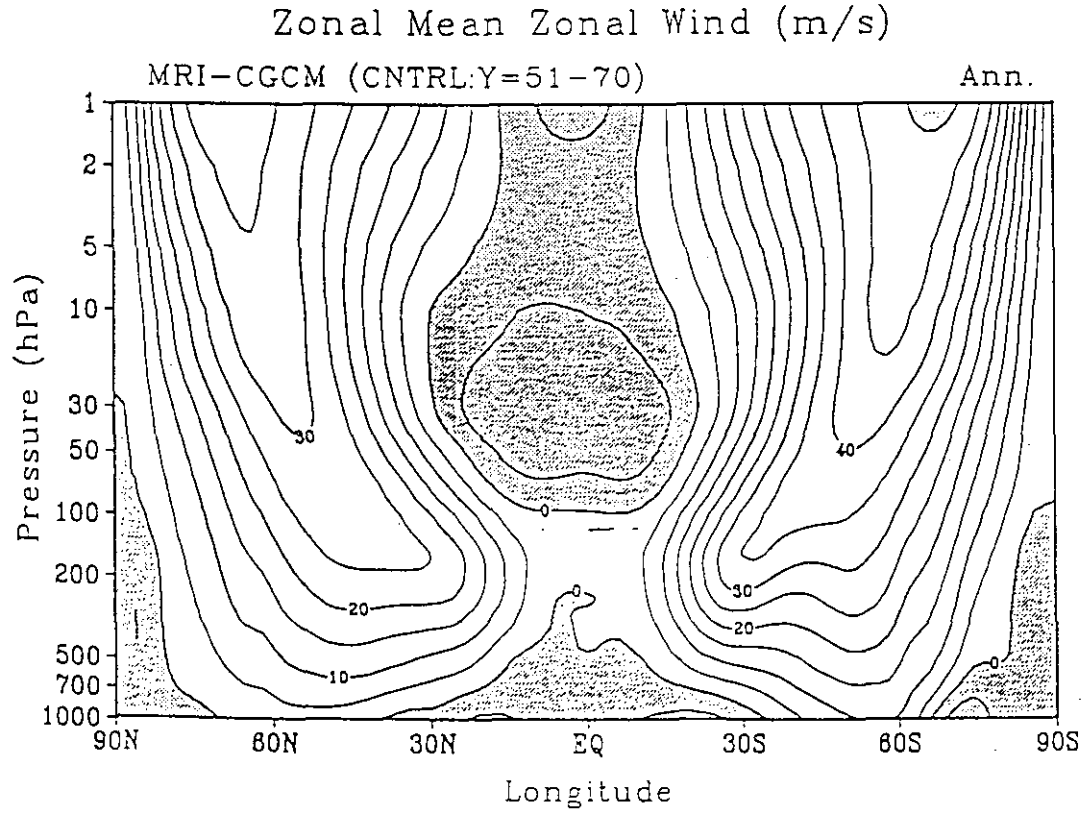

Fig. 11 As in Fig. 10 but for zonal wind. Contour interval is 5 m/s.

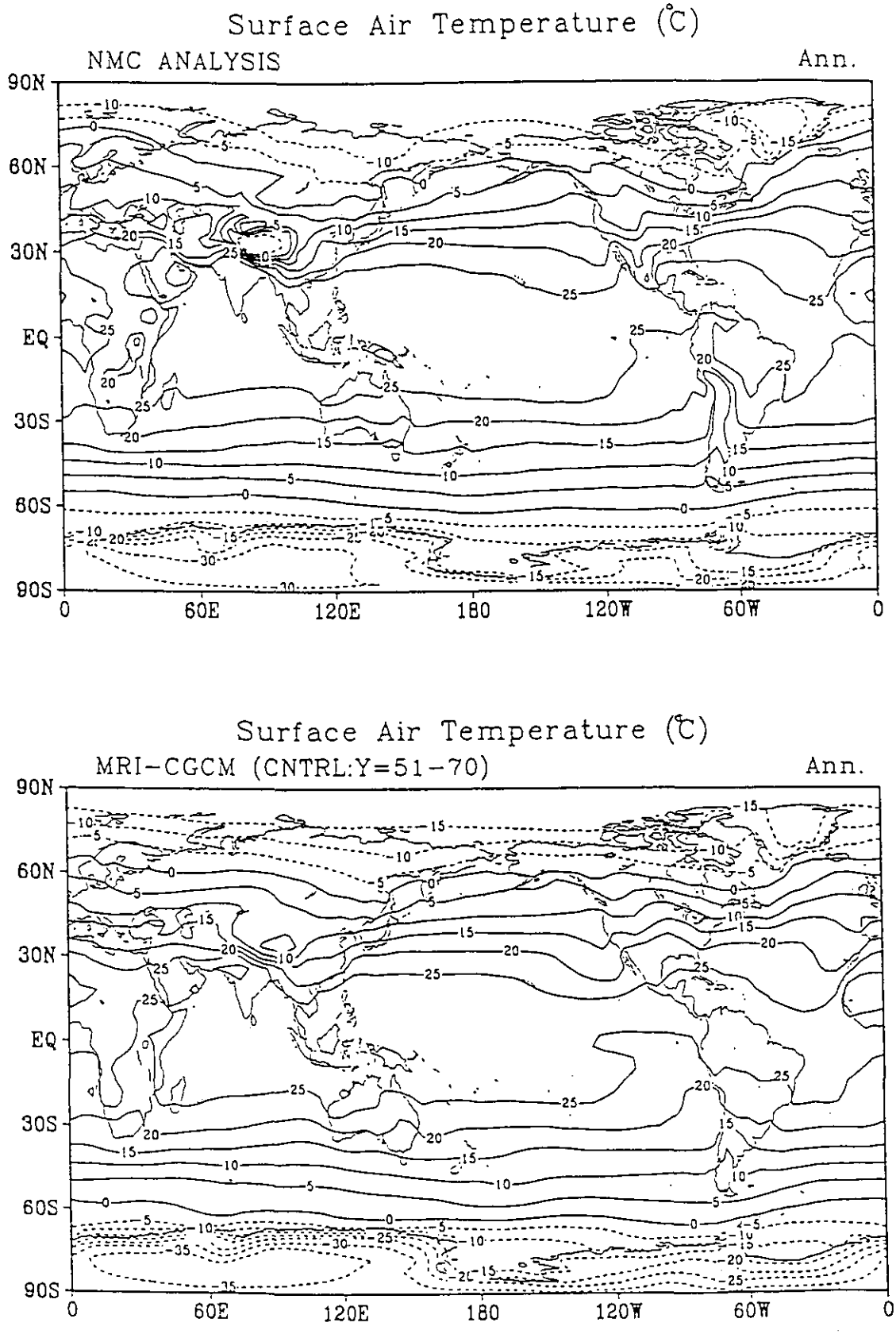

Fig. 12 Annual mean surface air temperature for observation from NMC analyses (upper panel) and for the C run (mean of years 51-70) (lower panel). Contour interval is 5°C.

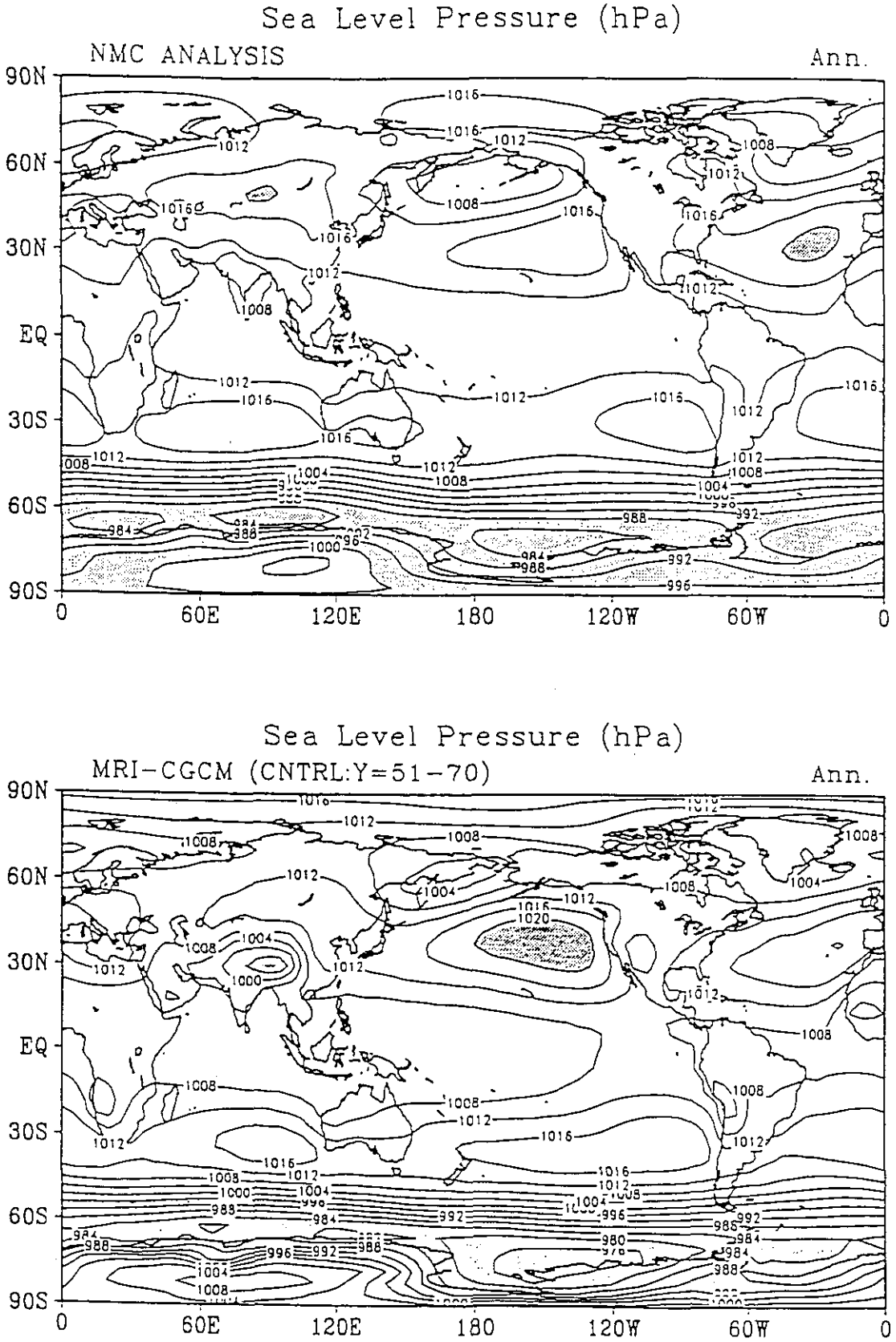

Fig. 13 As in Fig. 12 but for sea level pressure. Contour interval is 4 hPa.

basic features of the precipitation pattern for the C run (Fig. 14) are very similar to those obtained from the AMIP simulation and hence the biases are also similar, although the SST from the C run has a warm bias in the warm water regions of the tropics (see Fig. 8).

4.3 Sea ice

The simulated distributions of sea-ice concentration for March and September in the Northern Hemisphere (Fig. 15) were averaged over the last 10 years (years 61-70) of the control integration. In a comparison of the simulated distribution with the observed, the lack of penetration of warm water into the northern North Atlantic in the model results in sea ice covering the Greenland and Norwegian seas. The simulated distributions in the Arctic Ocean, the Sea of Okhotsk and the Bering Sea are similar to the observed distributions and show realistic seasonal variations. Though polynyas and light-ice areas are produced in the Southern Hemisphere by the model for September, the position of the simulated sea-ice edge is almost the same as that observed in both March and September (Fig. 16).

The seasonal variations of the simulated sea-ice thickness and snow depth were averaged over the last 10 years (years 61-70) of the control integration for the selected points in the Northern (0°E, 86°N) and Southern (0°E, 62°S) Hemispheres (Fig. 17). The selected point in the Northern Hemisphere is located within the multi-year sea ice region in the Arctic Ocean. The simulated sea-ice thickness for this point was above 2.4 m throughout the year, varying seasonally around the annual mean value of about 3 m (see Fig. 17a). The simulated snow over the sea ice melts annually beginning in May and disappears completely in July (see also Fig. 17a). These simulated seasonal variations of sea-ice thickness and snow depth are almost identical to those estimated by Maykut and Untersteiner (1971). Wadhams et al. (1987) observed that sea-ice thicknesses around the selected point in the Southern Hemisphere were 0.4 - 0.6 m from July to September in 1986. The simulated sea-ice thicknesses for this point during these months were 0.4 - 0.8 m (see Fig. 15b), which essentially agrees with observations.

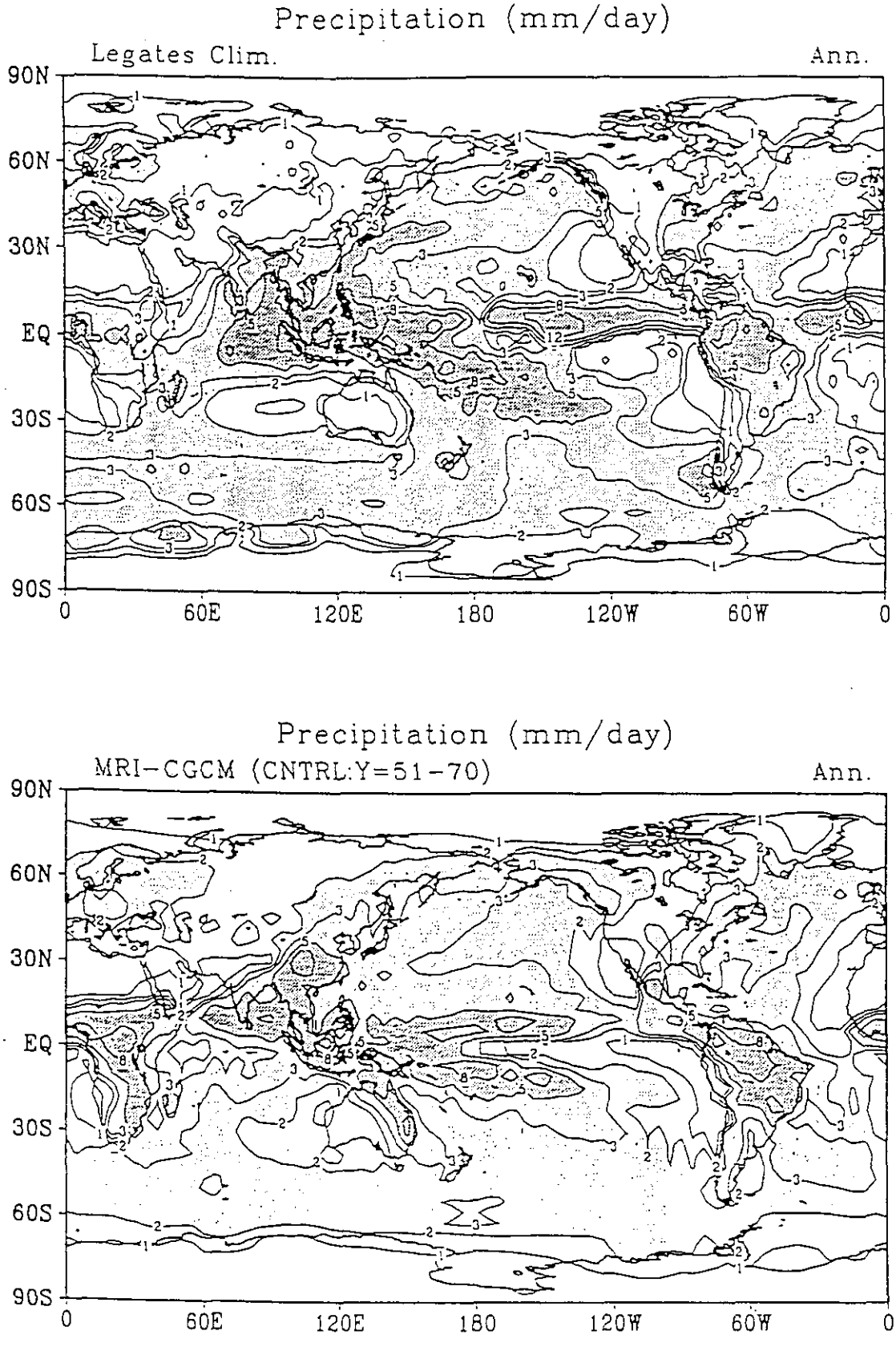

Fig. 14 As in Fig. 12 but for precipitation and observations (Legates, 1987). Contours for 1, 2, 3, 5 and 8 mm/day are drawn.

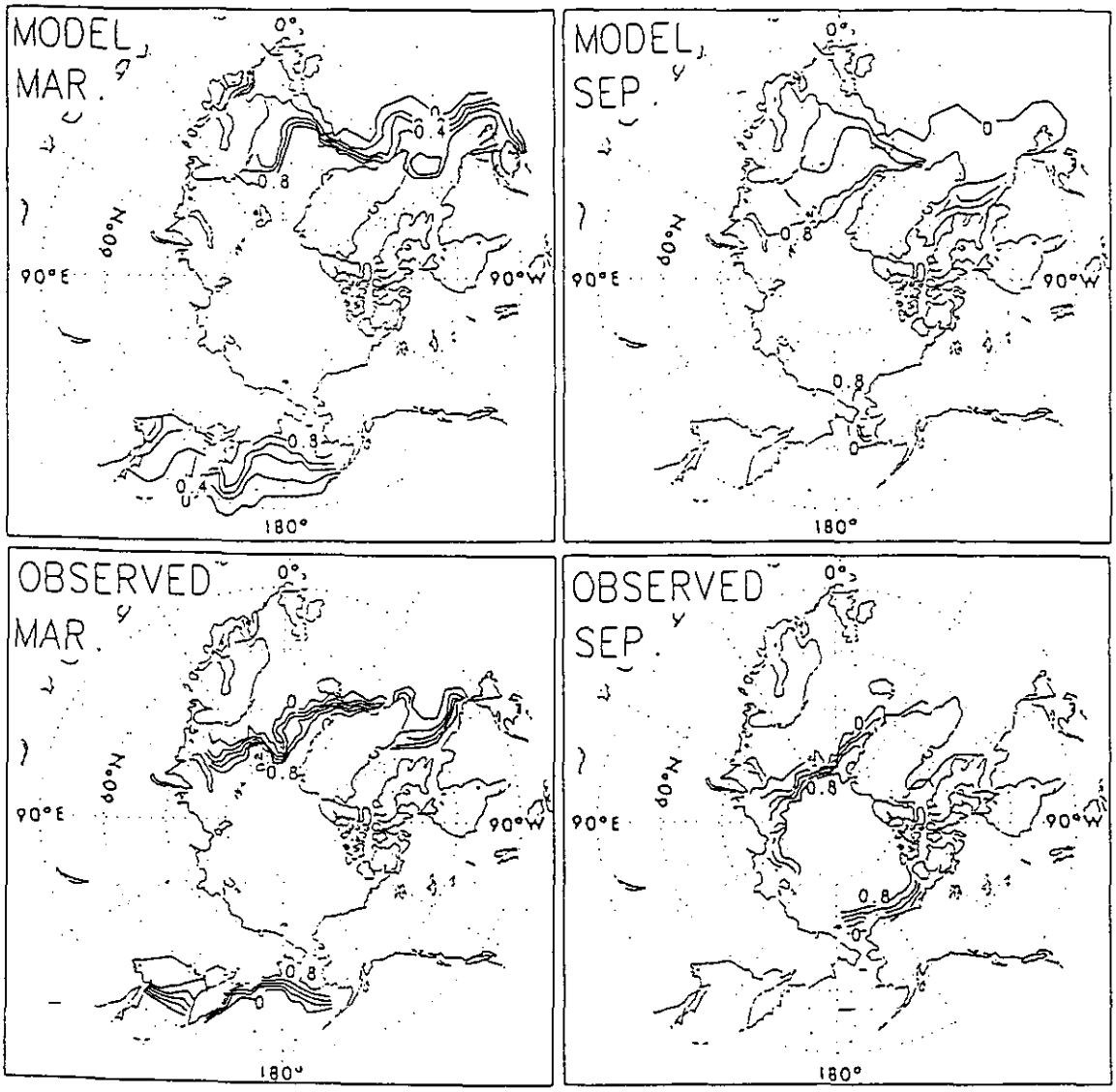

Fig. 15 Distributions of sea-ice concentration (proportion of coverage) for March (left) and September (right) in the Northern Hemisphere. Simulated values (upper panel) averaged over the last 10 years (61-70 year) of the C run and observed values (lower panel). The contour intervals are 0.2.

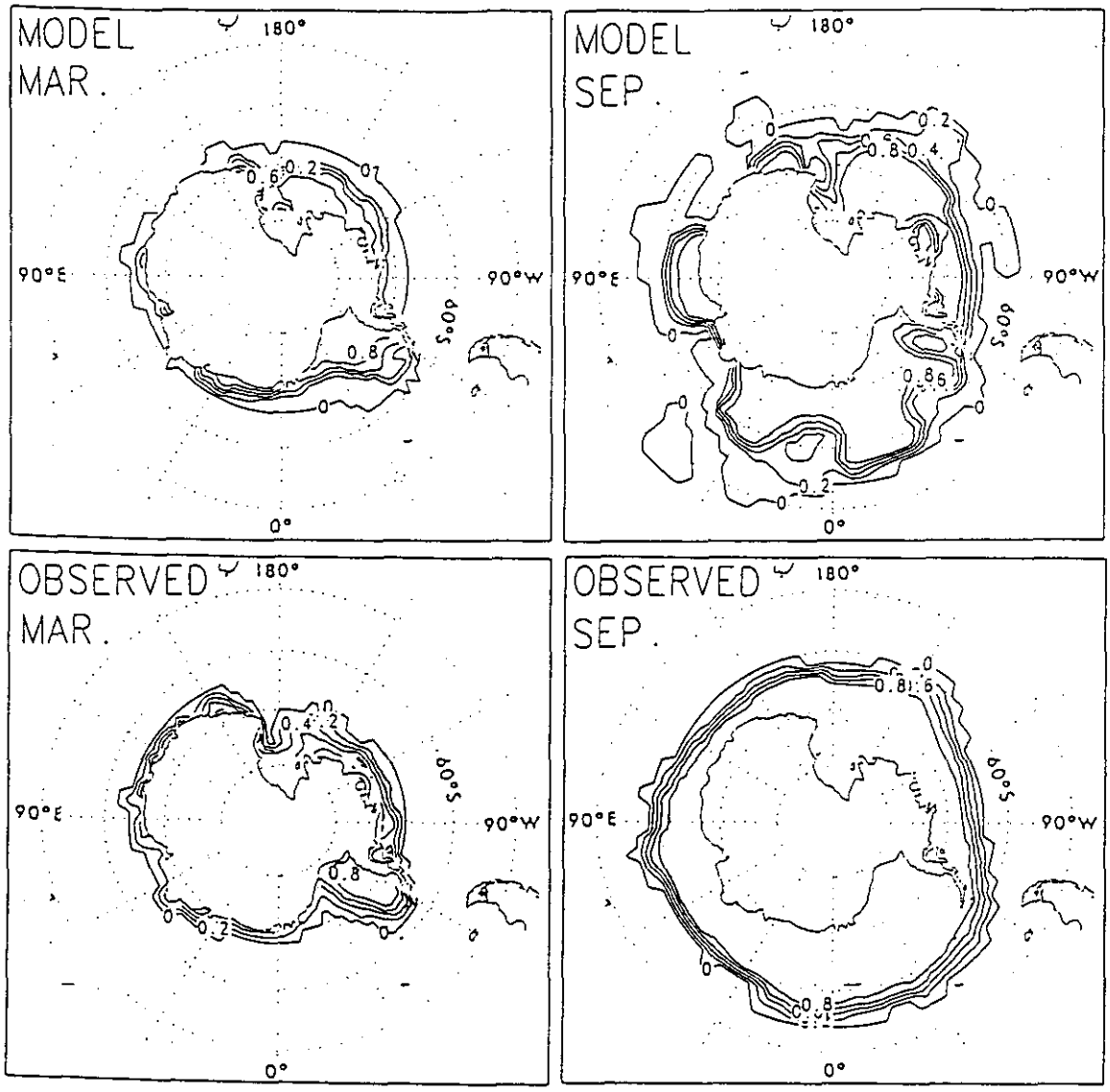

Fig. 16 Distributions of sea-ice concentration for March (left) and September (right) in the Southern Hemisphere. Simulated values (upper panel) averaged over the last 10 years (61-70 year) of the C run and observed values (lower panel). The contour intervals are 0.2.

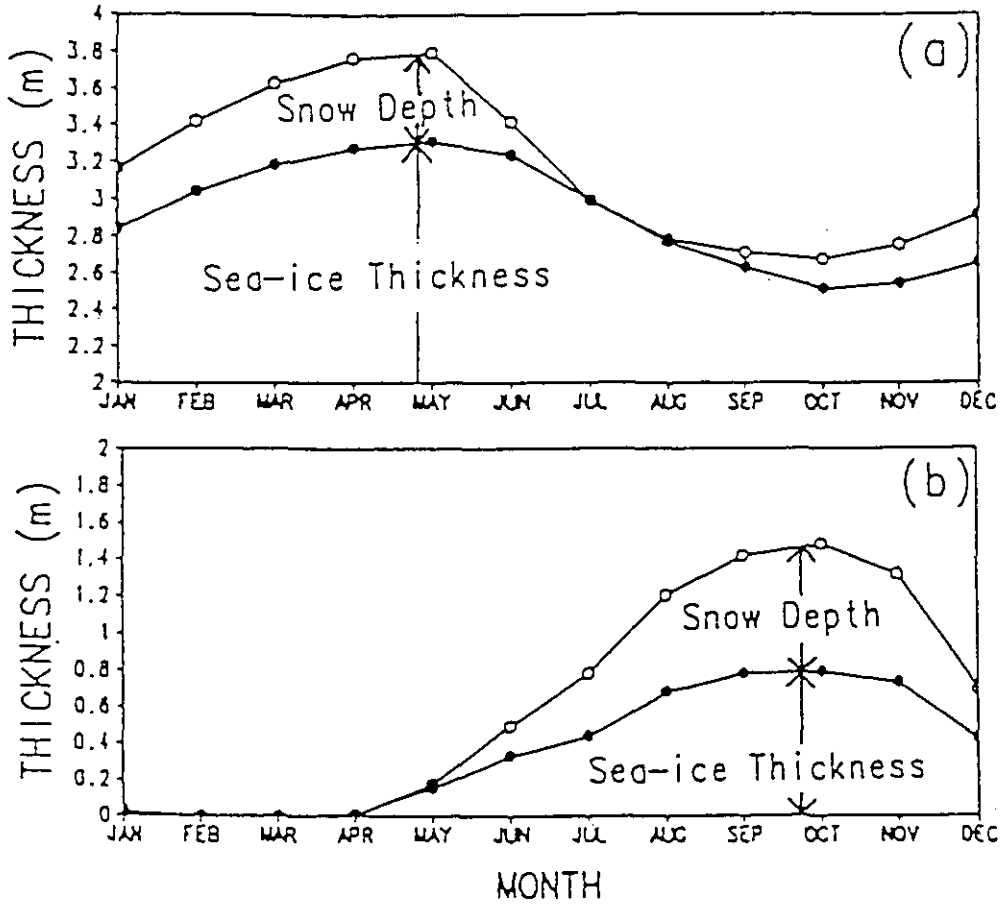

Fig. 17 Seasonal variations of the simulated sea-ice thickness and snow depth (a) for 0°E, 86°N and (b) for 0°E, 62°S, averaged over the last 10 years (61-70 year) of the C run.

4.4 ENSO and interdecadal variations

The simulated southern oscillation index (SOI), defined as the sea level pressure difference between Tahiti and Darwin, and the time series of the SST monthly anomaly at the NINO3 region (150°W-90°W, 10°S-10°N) (Fig. 18) show significant interannual oscillations with dominant periods of 3 to 6 years. The magnitude of the SST anomaly is larger than that obtained from the CGCM by Nagai *et al.* (1992), although it is still small compared to the observed peak value of 3°C. Time series of the model SOI also shows interannual variation which has a negative correlation with the SST anomaly of -0.72. This correlation is comparable with that for observed ENSOs. Moreover, a detailed analysis by Yukimoto *et al.* (1995) shows that the simulated ENSO has many similarities with observed ENSOs.

The most typical SST spatial variation pattern is extracted by empirical orthogonal function (EOF) analysis. The first EOF of SST for the C run (Fig. 19) has large amplitudes in the Pacific. The most notable feature of this mode is a wedge-like pattern in the central Pacific of opposite polarity in the north-western and the south-western mid-Pacific. The coefficient of the EOF shows dominant 6-year cycles (see Fig. 19), which are close to the typical time scale of El Niño events and their interdecadal modulations of about 30 years.

The first EOF of the annually averaged SST data, which are combinations of the COADS data for before 1985 and the JMA analyses for after 1986 (Fig. 20), has several characteristic features in common with those of the EOF analysis of the SST from the C run. There is a jump in the amplitude of the first EOF mode in the latter half of 1970s. Before this period, it remained negative. However, it remains positive thereafter. The above-normal SST in the eastern equatorial Pacific and the below-normal SST in the Northern mid-Pacific observed in recent years are captured by this mode.

Thus the above results suggest that the MRI-CGCM can simulate the main features of ENSO-scale to interdecadal variations.

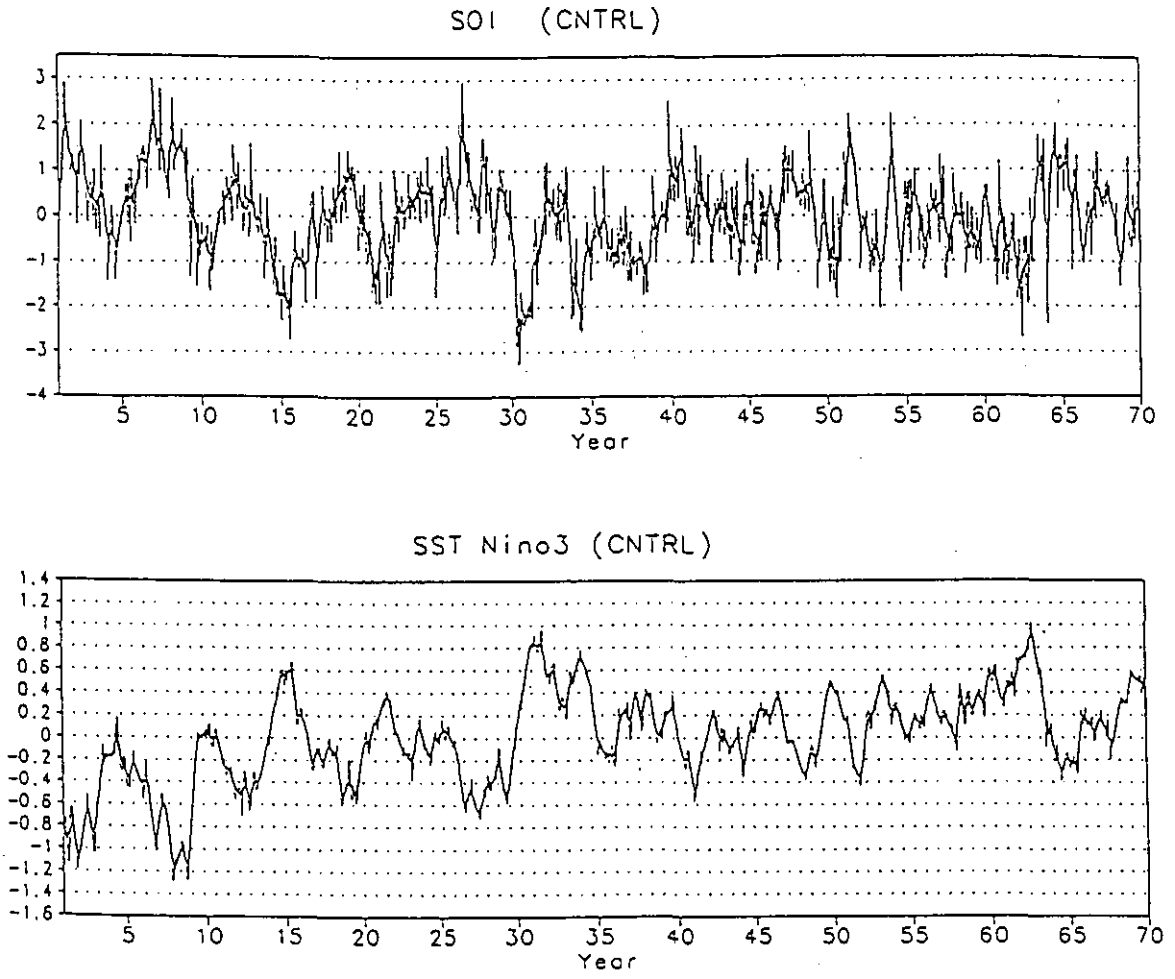

Fig. 18 Time series of simulated (upper panel) southern oscillation index (SOI) and (lower panel) SST anomaly in the NINO3 region (150°W-90°W, 10°S-10°N).

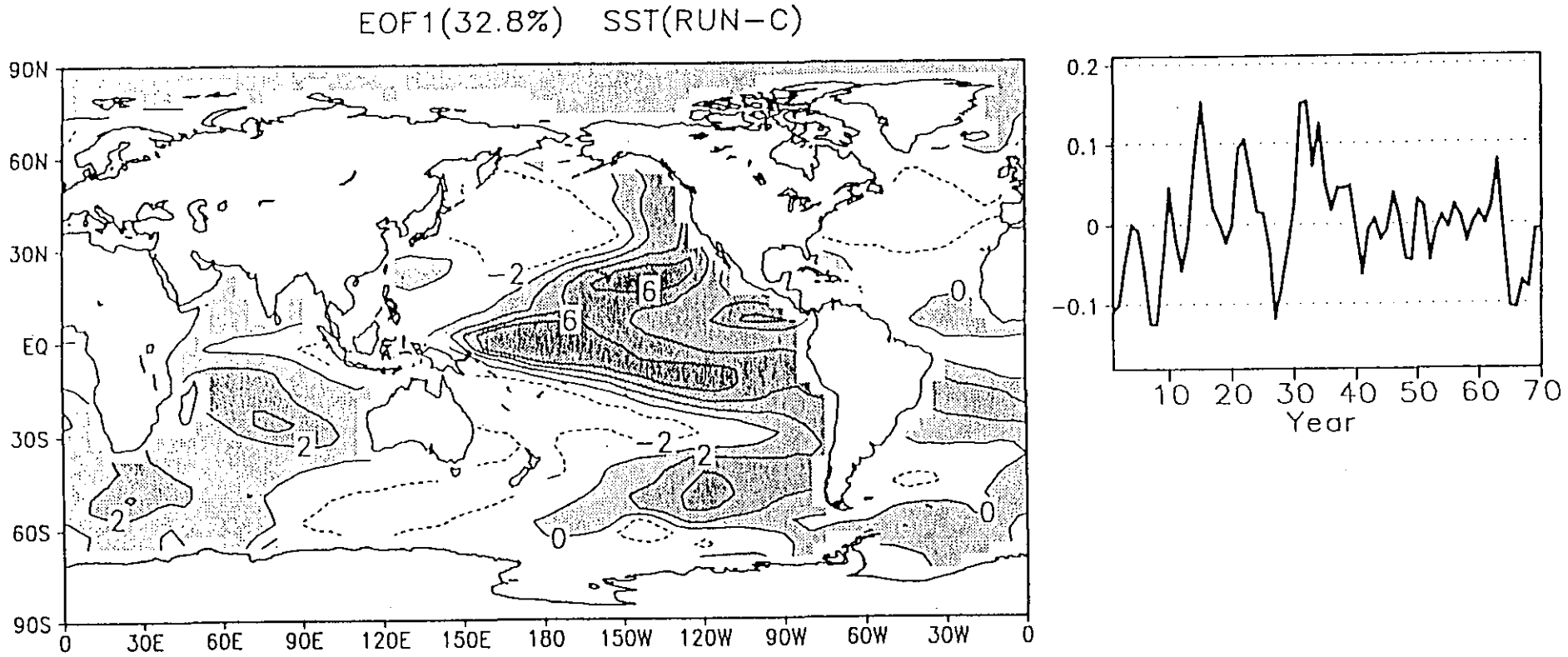

Fig. 19 The first mode of an empirical orthogonal function (EOF) analysis of the annually averaged SST for the C run. (left) Spatial pattern, (right) time evolution of the amplitude of the mode. Periods shorter than 12 years have been filtered out. The contribution of this mode to total variability is shown in the parentheses at the top of the figure.

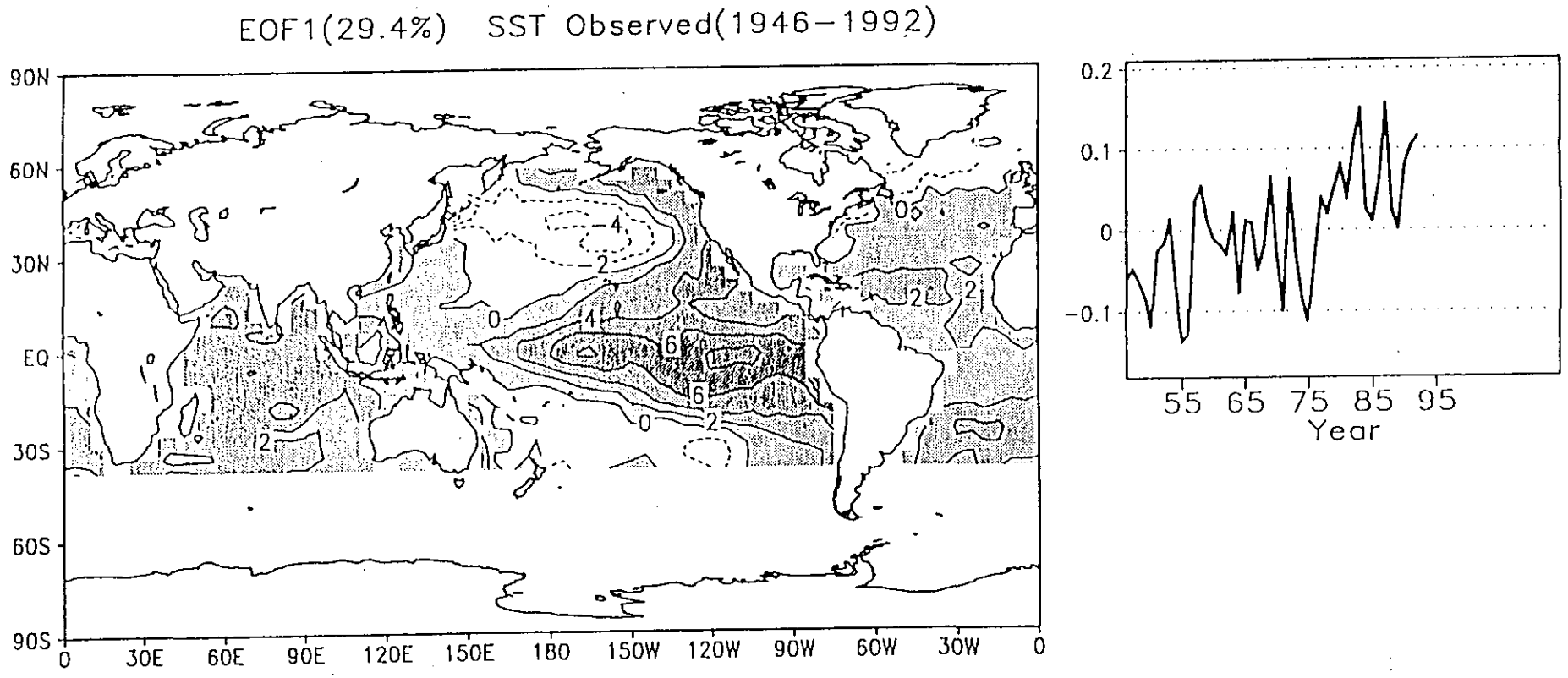

Fig. 20 The same as in Fig. 19 but for the first EOF for the observed SST, which is a combination of COADS data from 1946 to 1985 and the JMA analysis from 1986 to 1992.